



Feasibility study of geothermal heat extraction from abandoned oil wells using a U-tube heat exchanger

Shabnam Gharibi ^a, Emad Mortezaee ^a, Seyed Jalaledin Hashemi Aghcheh Bod ^b, Ali Vatani ^{b,*}

^a Institute of Petroleum Engineering, School of Chemical Engineering, College of Engineering, University of Tehran, Islamic Republic of Iran

^b School of Chemical Engineering & Institute of LNG, College of Engineering, University of Tehran, Islamic Republic of Iran

ARTICLE INFO

Article history:

Received 22 June 2017

Received in revised form

5 February 2018

Accepted 2 April 2018

Available online 10 April 2018

Keywords:

Geothermal energy

Numerical simulation

U-tube

Heat exchanger

Abandoned oil wells

Heat transfer

ABSTRACT

The purpose of this study is to demonstrate the feasibility of using an abandoned oil well as a geothermal resource. A three-dimensional numerical model of a U-tube heat exchanger is simulated based upon the real field data of an abandoned oil well located in southern Iran. To assess and optimize the performance of the heat exchanger, the influences of mass flow rate, fluid inlet temperature, insulation length, and pipe diameter are analyzed. The simulation results indicate that the retrofitted well can be utilized for both electricity generation and direct applications. The great advantage of the proposed heat exchanger is that it can work steadily as a long-term geothermal production system. In a case with 288.16 K inlet temperature and 0.03 m/s inlet velocity, the outlet temperature reaches 324.73 K at the first year of operation and it declines to 324.13 K after 5 years.

© 2018 Elsevier Ltd. All rights reserved.

1. Introduction

In view of rising energy demands, declining fossil energy sources and their adverse effects on the environment, the development and utilization of renewable energy resources is imperative for the near future. Geothermal energy is a promising alternative to fossil fuels due to the reliability, high availability [1], and most importantly being environmentally friendly [2]. These underground reservoirs of steam and hot water can be used for electricity production, direct usage and heat pump applications based upon the state of the extracted geothermal fluid and its temperature. The global electricity production in the geothermal power plants has increased from 1300 MW in 1975 to 10,715 MW in 2010 [3,4] and it is expected to reach over 40 GW by 2035 [5]. Unfortunately, the application of geothermal systems has been restricted owing to the high cost of well drilling. There are about 20–30 million abandoned oil wells throughout the world [6]. Using these wells instead of drilling new geothermal wells is an economically viable solution which can decrease the capital cost of the geothermal projects by

up to 50% [7]. Another significant reason for retrofitting the abandoned wells is the availability of geophysical well logs and geological studies on the existing wells. Furthermore, the problems of reinjection, corrosion and scaling can be eliminated given the fact that the circulating fluid is not in direct contact with the formation [8]. Researchers at the Leduc Energy Discovery Center seek to extract heat from the abandoned wells in Alberta. They concluded that the cost to abandon a disused well could be up to \$300,000 while converting it to geothermal and utilizing it for greenhouse operations could half that cost [9]. The abandoned oil wells are considered as a medium-to-low-temperature resource, which is a precious source of renewable energy [10]. Hence, several researchers have focused on the exploitation of geothermal energy from abandoned oil wells (e.g. Refs. [6–8,11–15]).

Kujawa et al. [11] assessed the possibility of extracting geothermal energy from an existing deep production well using a double pipe heat exchanger. The paper concluded that the fluid inlet temperature, flow rate and insulation on the inner pipe had a significant impact on the performance of the heat exchanger. Davis and Michaelides [12] proposed a numerical model of a double pipe heat exchanger retrofitted to an abandoned oil well. The effects of the down-hole temperature, injection pressure and flow rate of an organic working fluid were analyzed in this paper. Owing to the fact

* Corresponding author.

E-mail addresses: avatani@ut.ac.ir, dr.vatani@gmail.com (A. Vatani).

that the ground temperature was assumed constant with time, the calculated power output was overestimated. Bu et al. [7] developed a mathematical model describing the heat transfer between the well and the stratum, and concluded that the performance of the double pipe heat exchanger adapted to an abandoned oil well depends upon the fluid flow rate as well as geothermal gradient. Cheng et al. [13] performed a numerical simulation for an abandoned oil well with a depth of 6000 m. The results showed that the fluid outlet temperature gradually decreased with the system operating time and eventually approached stability. Furthermore, there was an optimal inlet velocity of fluid entering the injection well to maximize the net power for a specified geothermal heat source. Noorollahi et al. [14] investigated a 3D simulation of two abandoned oil wells based upon the real field data, and concluded that in addition to the mass flow rate and geothermal gradient, well casing geometry had a significant influence on the heat transfer in the wells and net electricity production. Alimonti and Soldo [8] studied the optimization of a wellbore heat exchanger embedded in one of the largest European oil fields. They considered the use of two different working fluids (i.e. water and diathermic oil) and different internal diameters of the pipes in the simulation. The results indicated that the extracted heat could be used either for district heating or for electricity production with an organic Rankine cycle machine. Cheng et al. [6] studied the effects of thermal reservoirs on geothermal power generation using abandoned oil wells. Therefore, they proposed a novel heat transfer model coupling 2-D thermal reservoirs with 1-D wellbore. The results showed that the thermal reservoirs can enhance the geothermal utilization efficiency of the abandoned oil wells. In addition, the thermal reservoirs parameters would significantly affect the heat production and power generation. Caulk et al. [15] investigated the suitability of abandoned oil and gas wells in California for enhanced geothermal systems and low temperature deep borehole heat exchanger applications. The paper concluded that the outlet temperatures above 40 °C can be easily acquired in areas with high geothermal gradients (7 °C/100 m) using a coaxial borehole heat exchanger installed in wells with depths > 1250 m. On the other hand, in regions characterized by temperature gradients lower than 4.5 °C/100 m, this target outlet temperature can only be obtained with well depths of 3000–5000 m. They mentioned that lower production temperatures (<40 °C) can also be coupled with a heat pump for general space heating applications.

A U-tube downhole heat exchanger retrofitted to a borehole is the most common method used to harness the ground heat for space conditioning [16,17]. Hence, a number of studies have been conducted on the design and performance of vertical U-tube heat exchangers for the utilization of shallow geothermal energy (e.g. Refs. [16,18–22]).

Li et al. [18] proposed a three-dimensional unstructured finite volume model for a ground-coupled heat exchanger and meshed the cross-section domain of the borehole using the Delaunay triangulation method. Based upon the comparison of the model predictions and experimental data of the fluid outlet temperature, the prediction accuracy of the presented model was confirmed. Bouhacina et al. [20] presented a novel tube design, finned U-tube, as a geothermal heat exchanger and studied two numerical models of smooth and finned U-tube heat exchangers. The simulation results indicated that the fins applied to the inner surface of the inlet and outlet pipes enhance the performance of the heat exchanger. Dai et al. [21] established a three-dimensional unsteady model of a vertical U-tube heat exchanger. The heat transfer process between the inside and outside of the borehole under short-term heat

storage was analyzed. The researchers concluded that the longer the heat storage time, the larger the temperature difference between the borehole wall and the surrounding soil and the lower the temperature difference between the fluid in the U-tube and the borehole wall. Furthermore, at the same time, the variation in the temperature difference between the surrounding rock and the more distant boundary is not appreciable. Lyu et al. [22] established a three-dimensional steady state numerical model to couple the working fluid flow in a single U-tube heat exchanger with a geothermal fluid in the borehole. The effects of four parameters, including mass flow rate, degree of depth, length of the U-tube and temperature difference between working fluid and geothermal field on the performance of the heat exchanger was analyzed. The density and specific heat capacity of water changed with temperature, whereas its thermal conductivity and viscosity were assumed to be constant. Under the conditions in this paper, the outlet temperature increased approximately 4 K when the U-tube length was extended almost 1 m. Therefore, it was concluded that lengthening the U-tube is the most efficient and cost-effective method for the extraction of geothermal energy. Moreover, the results indicated that compared to the fluid outlet temperature, the heat extraction rate was more sensitive to the variation of the U-tube length.

It should be noted that there is no comprehensive study on the simulation of a U-tube heat exchanger installed in a deep abandoned oil/gas well based upon the real field data, including the geothermal gradient, well geometry and ground layers. Ghoreishi-Madiseh et al. [23] presented a 3D transient model to analyze the utilization of the U-tube heat exchanger in an abandoned oil well with a depth of 700 m and bottom hole temperature of 50 °C. The temperature and flow fields in the ground and within the water flowing through the heat exchanger were investigated using a finite volume discretization method. The paper concluded that the hydraulic conductivity of the heat exchange medium, its thermal conductivity and the heat extraction rate have a significant influence on the performance of the U-tube heat exchanger retrofitted to the abandoned oil well.

The main purpose of this paper is to demonstrate the possibility of using abandoned oil/gas wells as geothermal resources. A 3D numerical model of a U-tube heat exchanger is simulated using the Fluent CFD software [24], based upon the real data from an abandoned oil well located in Khuzestan province, southern Iran. Moreover, the effects of four parameters, including mass flow rate, fluid inlet temperature, insulation length, and pipe diameter on the performance of the geothermal heat exchanger are investigated.

2. Physical model

The model consists of a U-tube heat exchanger embedded deep in an oil well; the well is then filled with a proper filling material called grout (i.e. water) which makes the heat transfer between the tube and the ground possible. Cold water as a working fluid is injected into the well through the inlet of the U-tube and acquires the geothermal heat while flowing through the U-tube. The material of the pipes is stainless steel. A typical schematic diagram of a borehole with a U-tube heat exchanger is illustrated in Fig. 1. The abandoned oil well modeled in this study is located in Khuzestan province, southern Iran with a depth of 3861 m, 0.244 m diameter, 412.1 K bottomhole temperature, and average geothermal gradient of 31.1 °C/km. According to the in-situ collected data, the average of the ground surface temperature is 293.72 K and the ground temperature is considered to increase linearly from the surface to the

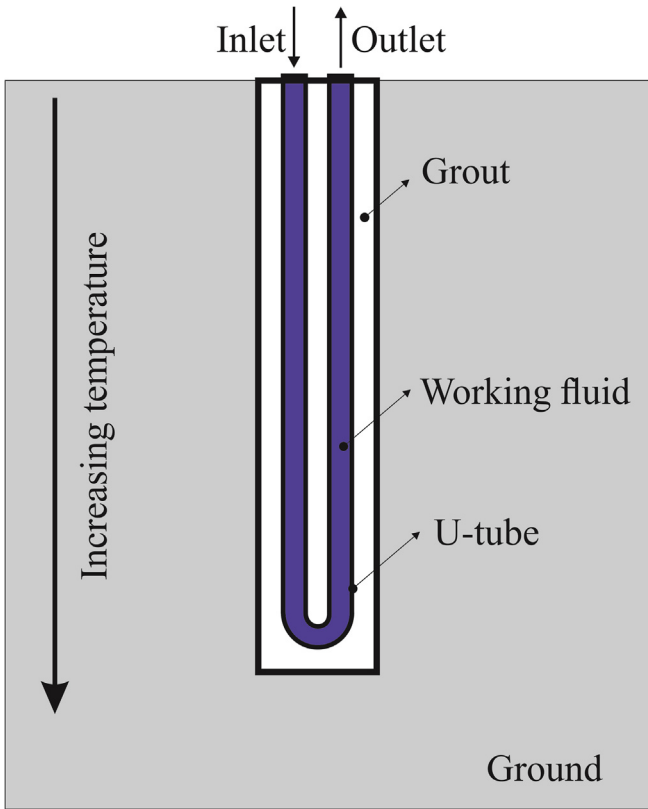


Fig. 1. Schematic diagram of a well with a U-tube heat exchanger.

bottom of the well. Well geometry, various ground layers and their thermo-physical properties are shown in Fig. 2, Tables 1 and 2, respectively.

3. Numerical model

In this paper, a three-dimensional numerical model in a Cartesian coordinate system is simulated. The first step to prepare the geometry of the model is constructing the U-tube (an elbow and two pipes), then the grout volume surrounding the U-tube, and finally the ground which encircles the entire computational domain. The generated volumes are meshed using Gambit, in which hybrid grid with the tetrahedron, hexahedron, prism and wedge element types are used. Meanwhile, owing to the importance of the grid size in near-wall treatment, boundary layers with the growth factor 1.2 are set. Furthermore, regarding the considerable well depth, the grid element numbers in the vertical or z direction are optimized to decrease both memory usage and computation time. Table 3 shows the simulation results of a U-tube heat exchanger with a length of 200 m for different grid numbers in the z direction. It can be seen that these four models give approximately the same results. Therefore, the grid size of 3 m along the z axis is applied to the following calculations in this paper.

It should be noted that both steady and unsteady state models have been simulated. According to the sensitivity study, in the steady state model, the optimum value of the ground radius is 6000 m and its depth is considered 2000 m higher than the well depth. However, the optimum ground radius for the unsteady state model is 300 m and its depth is 300 m higher than the well depth. The entire numerical model, including the U-tube heat exchanger, working fluid, grout and the surrounding ground consists of

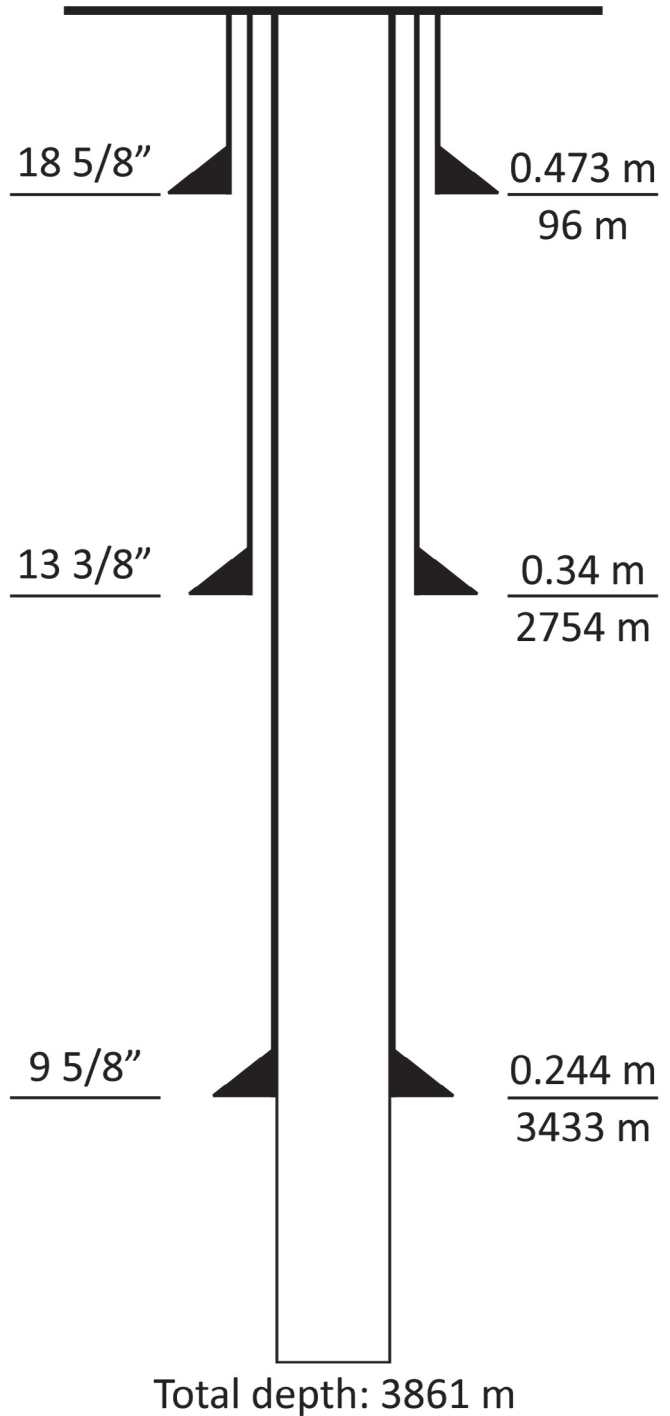


Fig. 2. Schematic diagram of the well geometry.

554605 and 465668 cells in the steady and unsteady models, respectively.

3.1. Governing equations

The entire simulation process is conducted using ANSYS Fluent software [24]. The CFD solver is based upon the finite volume method. The standard $k - \epsilon$ method is adapted to simulate the turbulent flow in the U-tube [25]. The pressure-velocity field is

Table 1
Depth of the different ground layers.

Layer index	Type of the layer	Depth (m)			Thickness (m)
		From	Middle	To	
1	Sandstone	0	1063	2127	2127
2	Marl	2127	2353	2579	452
3	Anhydrite	2579	2670	2762	183
4	Salt	2762	2846	2930	168
5	Limestone	2930	3023	3116	186
6	Marl	3116	3264	3412	296
7	Anhydrite	3412	3427	3443	31
8	Limestone	3443	3652	3861	418

coupled by SIMPLE algorithm. Shell conduction is applied on the borehole wall based upon the casing geometry, along with the U-tube walls, where the wall thickness is small in comparison with the overall geometry. The reason for this is that meshing these walls with solid cells would lead to high-aspect-ratio meshes and a significant increase in the total number of cells, and also computation time. It should be noted this option is only available when the pressure-based solver is selected. The first-order upwind discretization scheme is used for the convection terms of governing equations. The general equation for conservation of mass, or continuity equation, can be written as follows [24,26]:

$$\frac{\partial \rho}{\partial t} + \nabla \cdot (\rho \vec{v}) = S_m \quad (1)$$

The source S_m is the mass added to the continuous phase from the dispersed second phase and any user-defined sources. ρ and \vec{v} are the density and overall velocity vector, respectively. Conservation of momentum is described by Ref. [27]:

$$\frac{\partial}{\partial t}(\rho \vec{v}) + \nabla \cdot (\rho \vec{v} \vec{v}) = -\nabla p + \nabla \cdot (\bar{\tau}) + \rho \vec{g} + \vec{F} \quad (2)$$

where p is the static pressure, $\bar{\tau}$ is the stress tensor, and $\rho \vec{g}$ and \vec{F} are the gravitational body force and external body force, respectively. The stress tensor $\bar{\tau}$ is given by:

$$\bar{\tau} = \mu \left[(\nabla \vec{v} + \nabla \vec{v}^T) - \frac{2}{3} \nabla \cdot \vec{v} I \right] \quad (3)$$

where μ is the molecular viscosity, I is the unit tensor, and the second term on the right hand side is the effect of volume dilation. The energy equation is solved in the following form [24,26]:

$$\begin{aligned} \frac{\partial}{\partial t}(\rho E) + \nabla \cdot (\vec{v}(\rho E + p)) &= \nabla \cdot \left(K_{eff} \nabla T - \sum h_j \vec{J}_j + (\bar{\tau}_{eff} \cdot \vec{v}) \right) \\ &\quad + S_h \end{aligned} \quad (4)$$

where K_{eff} is the effective conductivity, and \vec{J}_j is the diffusion flux

Table 2
Thermo-physical properties of the geological layers and other simulation parameters.

Material	Density (kg/m ³)	Thermal conductivity (W/m K)	Specific heat capacity (J/kg K)
Sandstone	2300	2.64	873.62
Marl	2500	2.11	1036.64
Anhydrite	2960	0.5	856
Salt	1154	4.76	886.16
Limestone	2400	2.56	932.14
Stainless steel	8030	16.27	502.48
Water	998.2	0.6	4182

Table 3

The simulation results of a U-tube heat exchanger for different cell numbers in the z direction.

Cell numbers in the z-direction	400	200	100	66
Grid size in the z-direction (m)	0.5	1	2	3
Total cell numbers	7200	3600	1800	1188
Memory usage (MB)	58.49	55.81	48.28	46.91
Fluid outlet temperature (K)	299.24	299.22	299.21	299.19

of species j. The first three terms on the right-hand side of Eq. (4) represent energy transfer due to conduction, species diffusion, and viscous dissipation, respectively. S_h includes the heat of chemical reaction, and any other user-defined volumetric heat sources.

In Eq. (4),

$$E = h - \frac{p}{\rho} + \frac{v^2}{2} \quad (5)$$

where sensible enthalpy, h , is defined for incompressible flows as:

$$h = \sum_j Y_j h_j + \frac{p}{\rho} \quad (6)$$

Y_j is the mass fraction of species j, and:

$$h_j = \int_{T_{ref}}^T c_{pj} dT \quad (7)$$

where T_{ref} is 298.15 K.

The turbulence kinetic energy, k , and its rate of dissipation, ϵ , are given by the following transport equations [26,28,29]:

$$\begin{aligned} \frac{\partial}{\partial t}(\rho k) + \frac{\partial}{\partial x_i}(\rho k u_i) &= \frac{\partial}{\partial x_j} \left[\left(\mu + \frac{\mu_t}{\sigma_k} \right) \frac{\partial k}{\partial x_j} \right] + G_k + G_b - \rho \epsilon \\ &\quad - Y_M + S_k \end{aligned} \quad (8)$$

And

$$\begin{aligned} \frac{\partial}{\partial t}(\rho \epsilon) + \frac{\partial}{\partial x_i}(\rho \epsilon u_i) &= \frac{\partial}{\partial x_j} \left[\left(\mu + \frac{\mu_t}{\sigma_\epsilon} \right) \frac{\partial \epsilon}{\partial x_j} \right] + \left(C_{1\epsilon} \frac{\epsilon}{k} (G_k \right. \\ &\quad \left. + C_{3\epsilon} G_b) \right) - \left(C_{2\epsilon} \rho \frac{\epsilon^2}{k} + S_\epsilon \right) \end{aligned} \quad (9)$$

where S_k and S_ϵ are user-defined source terms, σ_k and σ_ϵ are the turbulent Prandtl numbers for k and ϵ . $C_{1\epsilon}$, $C_{2\epsilon}$ and $C_{3\epsilon}$ are empirical constants presented in Table 4. In terms of boundary conditions to solve Eqs. (1)–(9), velocity inlet and pressure outlet

Table 4

Turbulent constants in the $k - \epsilon$ equations.

$C_{1e} = C_{3e}$	C_{2e}	σ_k	σ_ϵ
1.44	1.92	1	1.3

are selected for the inlet and outlet pipes, respectively. To simulate the heat transfer, conduction is assumed to be the main mechanism in the ground and forced convection is considered as a dominant mechanism inside the U-tube. Unsteady heat transfer equation is solved in each time step to find temperature field in the ground and also in the grout and U-tube. Physical properties of water and ground layers are assumed to be constant.

4. Results and discussion

In order to investigate the performance of the U-tube heat exchanger retrofitted to abandoned oil wells in different years of operation and also the final rate of extracted heat, the simulations conducted under both steady and unsteady conditions. Furthermore, the sensitivity analyses on various model parameters, including fluid inlet velocity, its inlet temperature, insulation length applied to the outlet pipe and U-tube diameter were conducted to examine their effects on the performance of the heat exchanger. The parameters used in different models are presented in Table 5.

4.1. Steady state simulation

The results of the steady simulation show the final state of the model in which all the parameters reach stability. The criteria for convergence of the simulation are based upon the value of continuity, momentum, energy, κ and ϵ equations in residual forms. As shown in Fig. 3, 316 iterations are required to reach the defined small values of the residuals under the steady state condition.

In Fig. 4, the right side of the curves corresponds to the actual geothermal gradient of each geological layer, and the left side shows the temperature profile of the ground layers adjacent to the well. It is observed that the temperature of the ground layers surrounding the borehole rises as the ground radius increases up to 6000 m, and then it stays virtually constant. As shown in Fig. 5, the ground layer with higher thermal conductivity presents lower temperature variation with depth. For instance, the temperature gradient in the anhydrite layer with minimum thermal conductivity of 0.5 W/m K is much sharper than that in other layers. Moreover, the temperature difference between the inner and outer boundaries of a layer with higher thermal conductivity, is smaller than that of a layer with lower thermal conductivity. Considering the outlet pipe insulation from the top surface to the depth of 3700 m, the temperature variation in the limestone layer at 3700 m is justified. In other words, the ground temperature near the borehole wall at the depths where there is no insulation on the outlet pipe (i.e. 3700 through 3861 m) is slightly lower than the temperature of the upper zone in the limestone layer. The reason

for this is that the absence of insulation increases the heat transfer rate between the hot rock and the working fluid in the U-tube.

Fig. 6 illustrates the temperature profiles of the grout and working fluid with depth. The working fluid is gradually heated while flowing downward. In upward flow, the circulating water temperature increases as long as it is less than the grout temperature. Otherwise, the heat loss from the working fluid to the surrounding rock is inevitable. The temperature drop in the upward flow can be avoided by applying thermal insulation to the outlet pipe to a depth where heat transfer from water to the ground occurs. It can be observed that the steady state outlet temperature reaches 307.16 K with a velocity of 0.5 m/s at the inlet fluid temperature of 288.16 K resulting in 254.17 kW heat extraction rate. According to the temperature curve of the grout, at a special depth, the points with a lower temperature belong to the grid blocks near the inlet pipe and the ones with a higher temperature are related to the blocks adjacent to the borehole wall.

4.2. Unsteady state simulation

Fig. 7 shows the temperature profiles of the ground layers after 5 years of operation. It can be seen that the temperature drop around the well extends to the radius of 100 m, and then it stays almost constant. This value is significantly lower than the ground radius of 6000 m under steady state condition. Our study on the different models proves that considering the ground radius more than 300 m in the unsteady state simulation for 5 years of operation does not affect the results given that the temperature drop in the ground does not reach this radius. However, in the steady state simulation, the temperature drop extends to almost 6000 m. Considering the ground radius less than this value certainly affects the simulation results. The temperature profiles of the surrounding rock at the depth of 2846 m within 5 years of operation are shown in Fig. 8. The results indicate that the downward trend in the ground temperature will gradually slow down; hence it takes a long time to reach the steady state condition. The temperature-depth profile of the working fluid at different years of operation is presented in Fig. 9. In view of the decline in the circulating water temperature in downward flow with the passage of time, the fluid outlet temperature decreases. The reason for this is that the temperature difference between the ground and working fluid is reduced due to the temperature drop of the surrounding formations, leading to the decrease in the heat transfer rate as well as fluid outlet temperature. Moreover, as shown in Fig. 9, the maximum temperature drop occurs within the first year of operation, and then the outlet temperature reaches 316 K after 5 years, which is 8 K higher than that at steady state condition. It is also observed that the variation of the working fluid temperature with depth in the anhydrite layer (i.e. 2579–2762 m) is lower, because the temperature of the inner boundary at this layer is less than that at other ground layers.

4.3. Sensitivity analysis

The effects of a multitude of parameters on the performance of a

Table 5

Different parameters used in the simulations.

Parameter	Steady state simulation	Unsteady state simulation
Outer ground radius (m)	6000	300
U-tube diameter (m)	0.047	0.01, 0.02, 0.047
Insulation length (m)	3700	0, 1850, 3700, 3861
Fluid inlet temperature (K)	288.16	288.16, 293.16, 298.16, 303.16
Fluid inlet velocity (m/s)	0.5	0.02, 0.03, 0.5, 1.0, 1.5, 2.0, 2.5

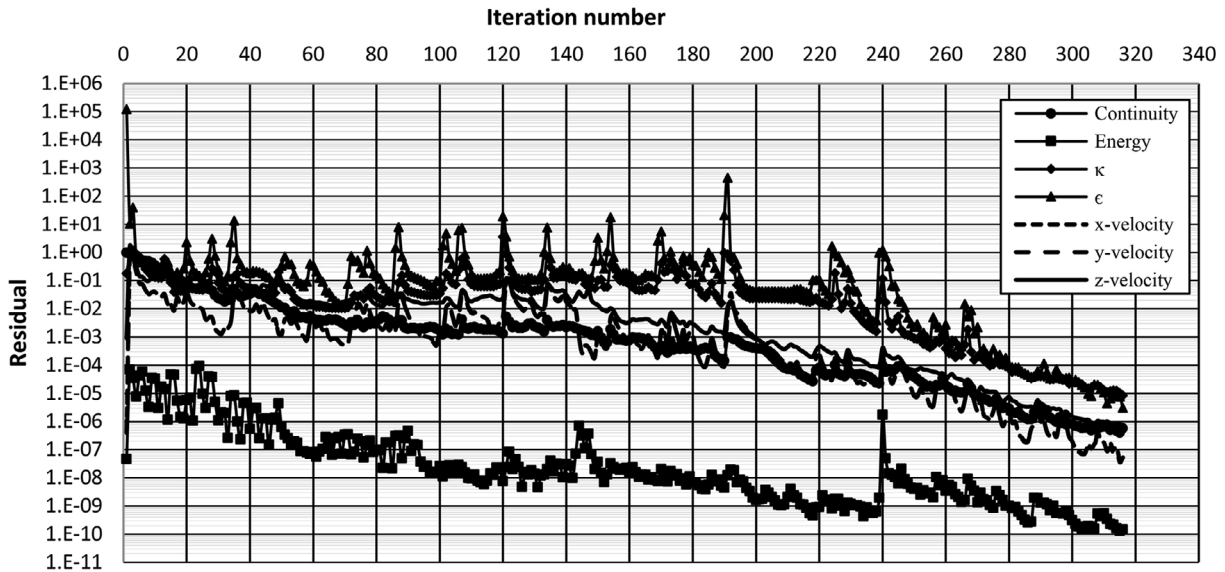


Fig. 3. The residual values of governing equations vs. iteration number for the steady state simulation.

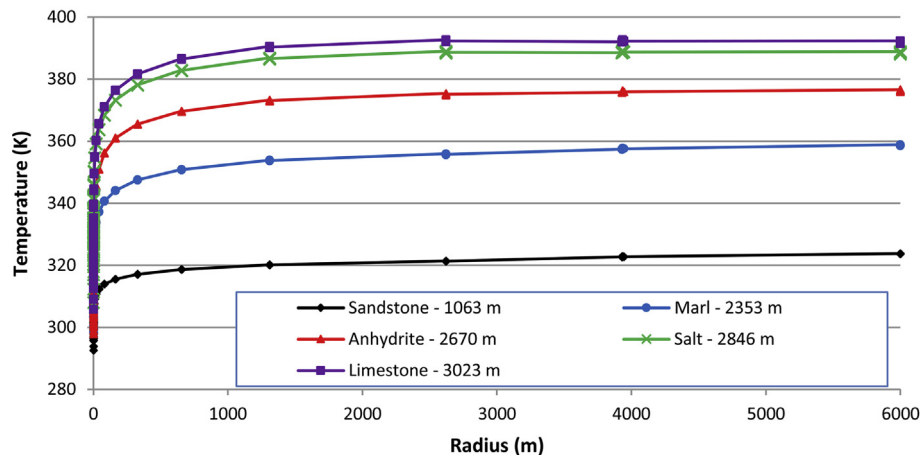


Fig. 4. Temperature variation of surrounding geological layers with ground radius in the steady state simulation at $U_i = 0.5 \text{ m/s}$ and $T_i = 288.16 \text{ K}$.

U-tube heat exchanger are investigated through a sensitivity study. The simulation results indicate that the highest outlet temperature is achieved at maximum inlet temperature of 303.16 K, and minimum inlet velocity of 0.5 m/s. On the other hand, the maximum gross heat power can be reached at the lowest inlet temperature of 288.16 K and the highest inlet velocity of 2.5 m/s. Consequently, sensitivity analyses of different variables, including fluid inlet velocity, inlet temperature, the length of the outlet pipe insulation and the U-tube diameter are performed for both cases mentioned above.

4.3.1. Working fluid inlet velocity

The mass flow rate increases with an increase in the fluid inlet velocity according to Eq. (10). On the one hand, based upon Eq. (11), the amount of the gross heat power rises with an increase in the mass flow rate once the enthalpy difference of the working fluid is considered constant; On the other hand, at high fluid inlet velocity, there is a relatively short time for the heat conduction between the circulating water and the hot wall of the U-tube, hence the fluid

outlet temperature will decrease. Furthermore, increasing the inlet velocity requires more hydraulic pressure, resulting in a higher amount of pumping energy. Fig. 10 presents the effect of different inlet velocities on the heat extraction rate and outlet fluid temperature. It should be mentioned that the flow regime inside the U-tube changes from laminar to turbulent at the velocity of 0.03 m/s. Therefore, as can be seen in the cited figure, the outlet fluid temperature peaks at 0.03 m/s inlet velocity with 1850 m of the insulation length on the outlet pipe and 288.16 K inlet temperature. Moreover, as expected, higher inlet velocities result in higher produced power and vice versa for lower inlet velocities.

$$\dot{m} = \rho A U \quad (10)$$

$$\dot{Q} = \dot{m}(H_2 - H_1) \quad (11)$$

As mentioned in advance, the velocity profile at the inlet section is flat as a defined boundary condition, then it gradually becomes dome-shaped, which is a characteristic of laminar flow for a velocity of 0.02 m/s with Reynolds number of 1870.6 (Figs. 11 and 12).

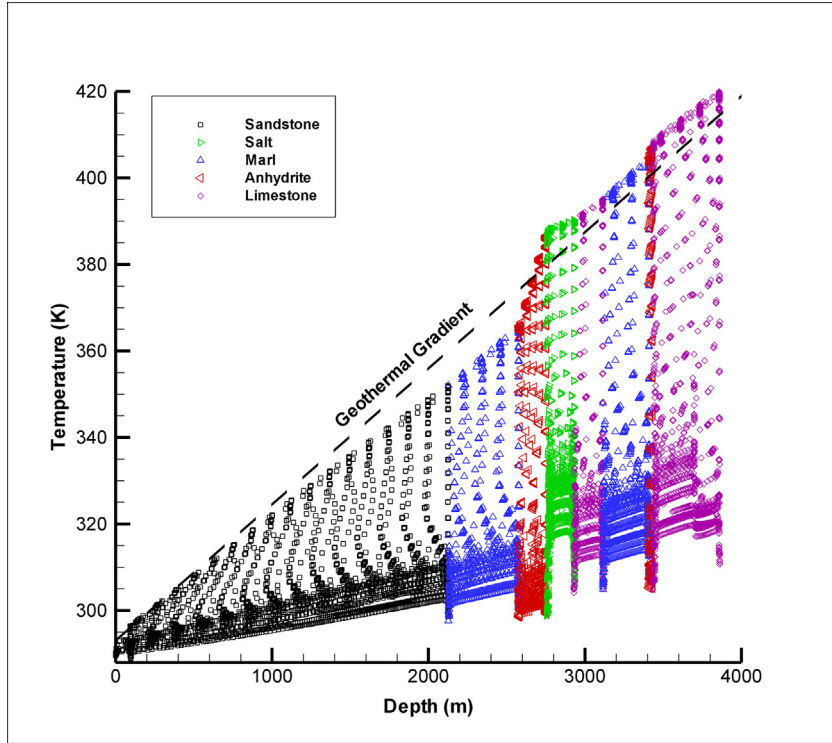


Fig. 5. Temperature variation of different ground layers with depth at $U_i = 0.5 \text{ m/s}$ and $T_i = 288.16 \text{ K}$.

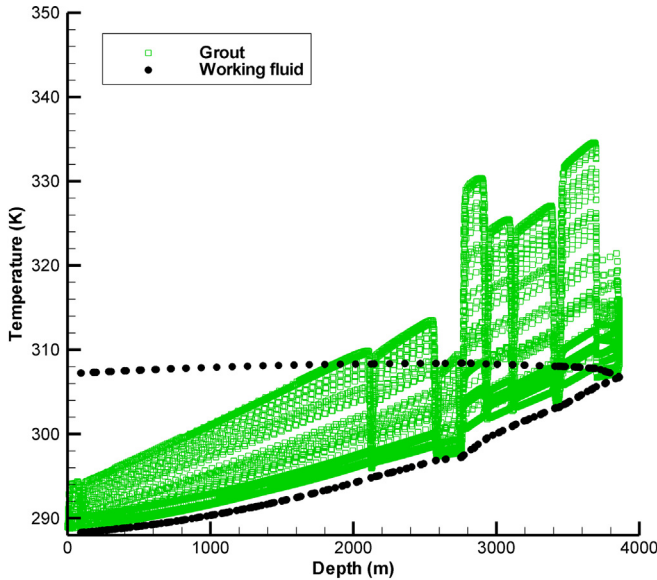


Fig. 6. Temperature variation of grout and working fluid along the U-tube heat exchanger at $U_i = 0.5 \text{ m/s}$ and $T_i = 288.16 \text{ K}$.

Fig. 13 presents the outlet velocity profile of the working fluid for 2 m/s inlet velocity, at which the flow regime is fully turbulent with Reynolds number of 187060. The points in the cited figures are the center of faces in inlet and outlet sides of the U-tube. The values of x-axis are the position of the points with respect to the origin of the coordinates of the entire model, which is set at the center of the wellbore. The velocity vectors at various cross sections are illustrated in Fig. 14.

4.3.2. Working fluid inlet temperature

Rising the inlet temperature results in decreasing the temperature difference between the well and working fluid in addition to the decline in the heat transfer from the ground to the working fluid. Results from the sensitivity analysis on different inlet temperatures are presented in Fig. 15. In this study, the ground surface temperature is considered constant at 293.72 K. As long as the inlet temperature is lower than the bottom-hole temperature, the outlet temperature will be greater than the inlet one. In addition, an increase in the inlet temperature causes the decline in the temperature difference between the inlet and outlet sections leading to the decrease in the produced heat power.

4.3.3. The length of the outlet pipe insulation

The thermal insulation used in this model is polystyrene with the thermal conductivity of 0.03 W/m K. In the downward flow, the water temperature rises steadily owing to increasing not only the U-tube temperature, based upon the geothermal gradient, but also the length of time that the fluid is in contact with the hot wall. In the upward direction, the grout temperature decreases until it becomes lower than the working fluid temperature at a particular depth. Thus, to avoid the fluid heat loss while ascending from this depth to the ground surface, it is essential to apply a thermal insulation to this length of the outlet pipe. The simulation results for both cases (i.e. maximum power output and maximum outlet temperature) during 5 years of operation are shown in Figs. 16 and 17. According to the curves, the heat exchanger produces the highest extracted power and outlet temperature at 1850 m insulation height. Moreover, it can be concluded that the optimal value of the insulation length is independent of both fluid inlet velocity and inlet temperature.

Figs. 18 and 19 demonstrate the temperature – depth profiles of the working fluid for two different input data after 5 years of operation. Decreasing the insulation length results in the heat

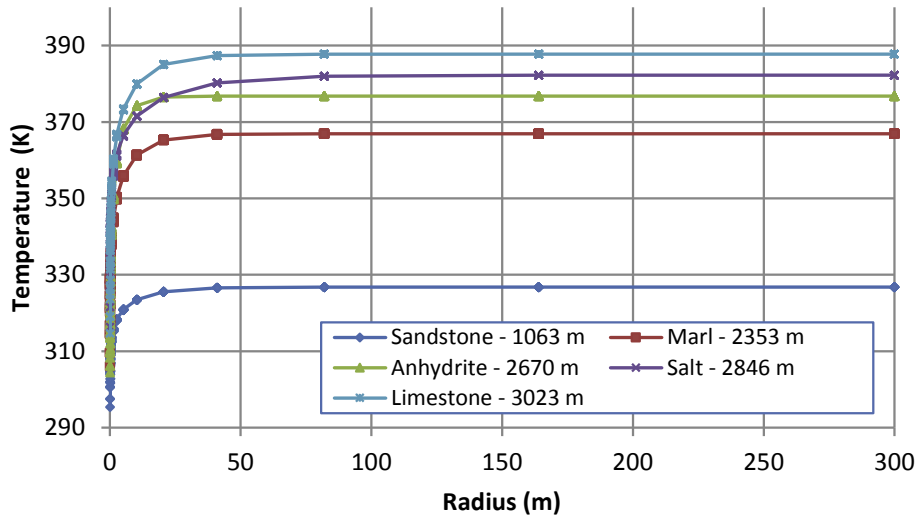


Fig. 7. Temperature variation of the surrounding ground with position after 5 years of operation at $U_i = 0.5 \text{ m/s}$ and $T_i = 288.16 \text{ K}$.

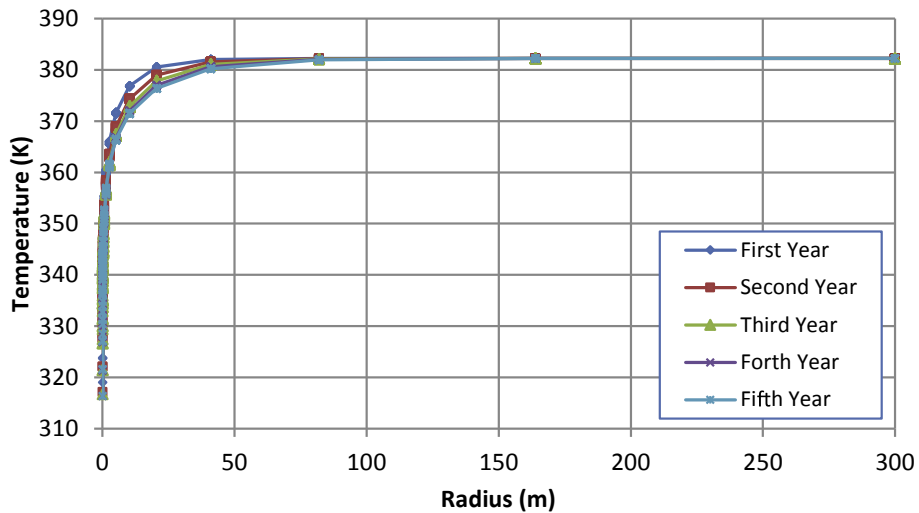


Fig. 8. Temperature variation of the surrounding rock with radius at 2846 m for different years of operation at $U_i = 0.5 \text{ m/s}$ and $T_i = 288.16 \text{ K}$.

transfer from the ground to the water in the upwind flow. However, without a thermal insulation, the downward flow is heated by the upward flow. Consequently, the ascending fluid temperature decreases while the descending fluid temperature increases. According to the figures cited above, it is concluded that the optimal value of the insulation length is 1850 m. In the blue curve, due to the absence of the insulator, along with the high rate of heat transfer at lower depths, the working fluid temperature increases and decreases at the inlet and outlet sections, respectively. This abrupt change is associated with the developing flow at the entrance length. In Fig. 18, owing to the high fluid velocity (i.e. 2.5 m/s), there is a relatively short time for the heat transfer from the U-tube wall to the working fluid. Moreover, the absence of insulation decreases the temperature difference between the ground and the circulating water, resulting in the lower heat transfer rate compared to the cases with thermal insulation. Therefore, the blue curve almost matches the red curve, regarding 1850 m insulation height, at higher depths. It should be considered that the high fluid velocity in the outlet pipe decreases the heat loss from the ascending fluid and causes the slight drop in its

temperature. The fluid velocity in Fig. 19 is much lower (0.5 m/s) than that in the case described above. Hence, in the absence of thermal insulation (i.e. the blue curve), due to the high rate of heat transfer from the working fluid to the surrounding grout, a sharp decline in the ascending fluid temperature can be observed. The amount of extracted gross power via the insulation length is shown in Fig. 20. It can be seen once more that the optimal value of the insulation height is 1850 m to achieve both purposes (i.e. maximum generated power as well as outlet temperature). The U-tube diameter.

Sensitivity analysis on different pipe radii is carried out based upon two distinct conditions; including constant inlet velocity and inlet mass flow rate.

4.3.3.1. Constant inlet velocity. Figs. 21 and 22 show the variation of the fluid outlet temperature and the extracted geothermal energy with pipe radius at the fifth year of simulation. It can be observed that increasing the pipe radius decreases the extracted working fluid temperature, but increases the amount of heat generated from the abandoned oil well. Doubling the pipe radius leads to a fourfold

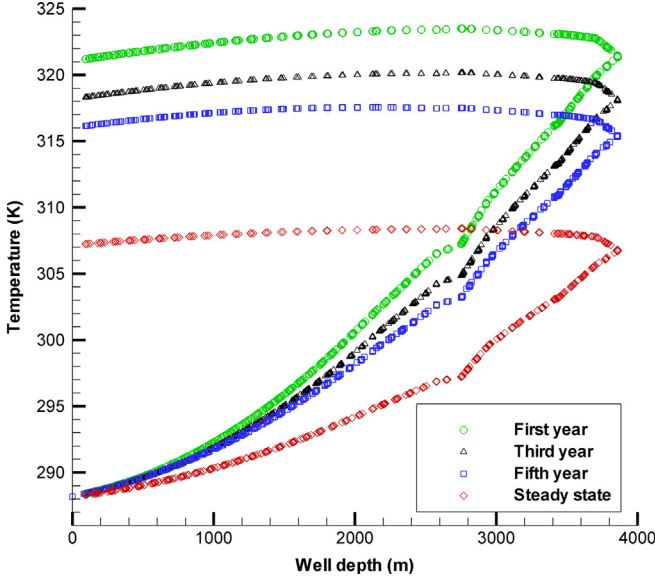


Fig. 9. Temperature variation of working fluid along the U-tube heat exchanger at different years of operation at $U_i = 0.5 \text{ m/s}$ and $T_i = 288.16 \text{ K}$.

increase in the mass flow rate in addition to a twofold increase in the amount of heat transferred from the U-tube wall to the working fluid, according to Eq. (12). Therefore, as illustrated in Fig. 23, a larger pipe radius will result in a lower temperature variation in the circulating water and also its outlet temperature. In the case of maximum outlet temperature, the fluid inlet temperature of 303.16 K is higher than the ground surface temperature (i.e. 293.72 K); hence, at the entrance length of the U-shaped heat exchanger, the heat transfer occurs from the working fluid to the ground, and the working fluid inlet temperature decreases as can be seen in Fig. 24. When the ground temperature becomes higher than the working fluid temperature, the heat transfer is reversed. Regarding the above reasons, the decrease and increase of the fluid temperature in the pipe with the smallest radius (0.01 m/s) is more noticeable than that with a higher radius.

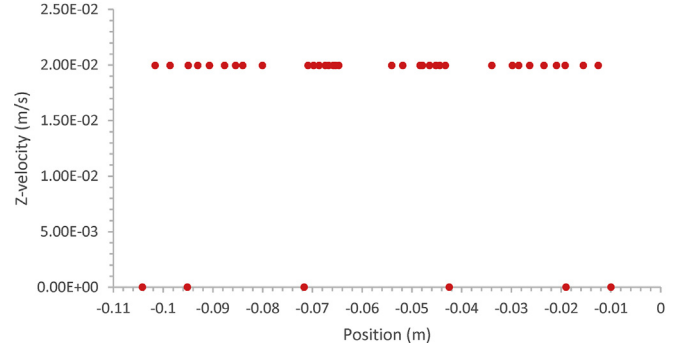


Fig. 11. Working fluid velocity at inlet section.

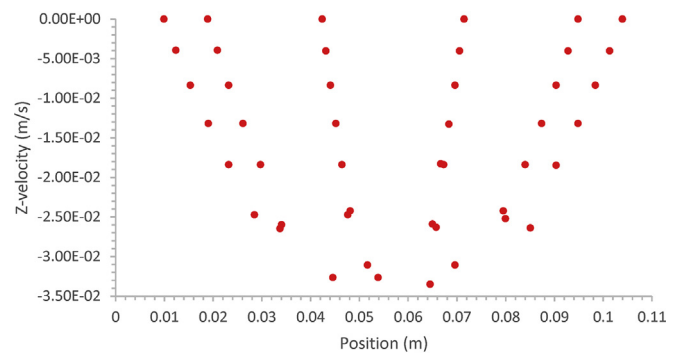


Fig. 12. Dome-shaped velocity profile of working fluid in laminar flow at outlet section.

$$\vec{q} = -k \vec{\nabla} T \quad (12)$$

More importantly, as shown in Fig. 25, the fluid outlet temperature does not appreciably change with time through 5 years of operation. In a word, the abandoned oil well studied in this paper can be utilized as a long-term geothermal resource either for electricity production or for direct applications using the U-tube heat exchanger.

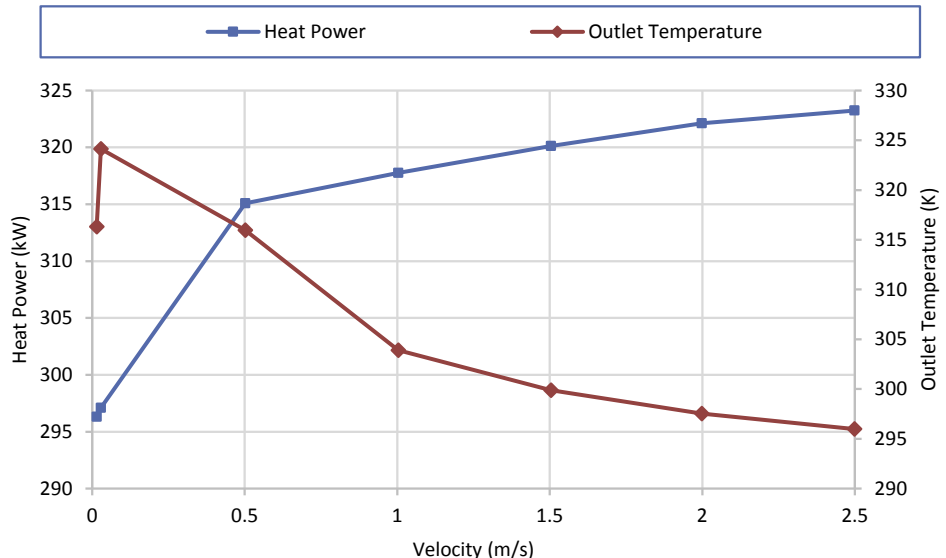


Fig. 10. Performance of the U-tube at different water inlet velocities at $T_i = 288.16 \text{ K}$.

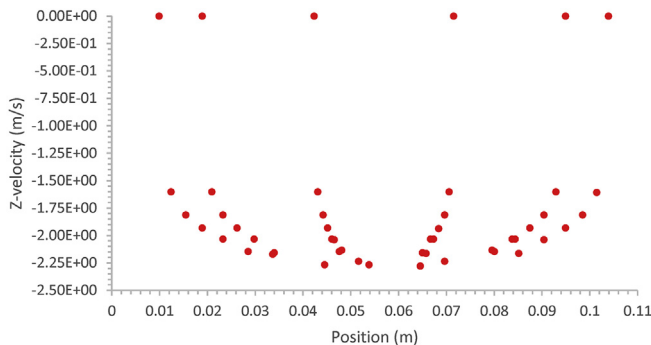


Fig. 13. Velocity profile of working fluid in turbulent flow at outlet section.

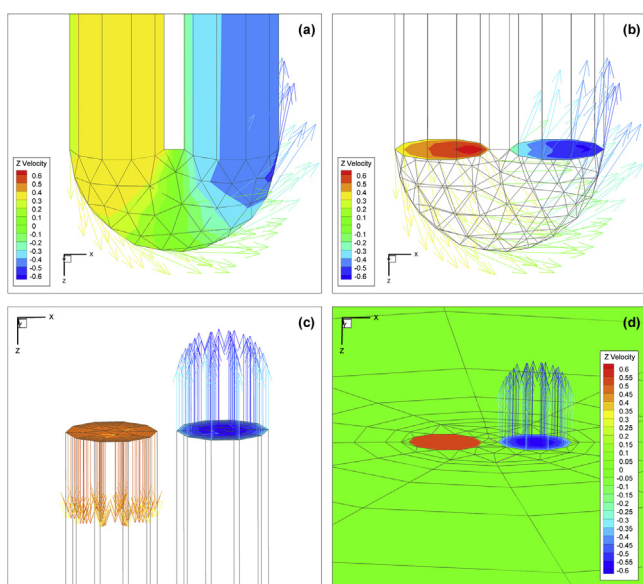


Fig. 14. Velocity vectors at different cross sections, a, b: velocity vectors in the elbow of the U-tube, c, d: velocity vectors in inlet and outlet sections of the pipes.

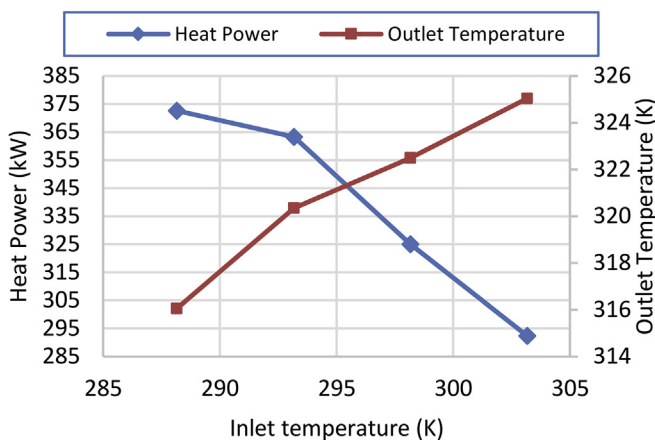


Fig. 15. Performance of the U-tube at different water inlet temperatures ($U_i = 0.5 \text{ m/s}$).

4.3.3.2. Constant mass flow rate. In this section, the simulation is conducted based upon the constant mass flow rate of 0.78 kg/s and different pipe radii. Eq. (11) shows a positive correlation between

the amounts of produced heat power and the working fluid outlet temperature when the mass flow rate and fluid inlet temperature are assumed constant. Fig. 26 illustrates the temperature variation of the working fluid with depth for different pipe radii. Rising the pipe radius at constant mass flow rate decreases the fluid velocity whereas increases the heat transfer surface between the U-tube wall and the circulating water. On the one hand, the two factors mentioned above increase the working fluid temperature as well as the heat transfer rate from the U-tube to the water in the downward direction; on the other hand, they will adversely affect the water temperature in the upward direction. Consequently, increasing the pipe radius at constant mass flow rate enhances the heat exchanger performance in the downward flow while reduces its efficiency in the upward flow. It can be concluded that based upon the amount of energy received in the downward flow and the amount of heat loss in the upward flow, the outlet temperature will have a positive or negative correlation with the pipe radius.

5. Conclusion

The present study demonstrates the feasibility of acquiring geothermal energy from an abandoned oil well retrofitted with a U-tube heat exchanger. The extracted thermal energy could be used for direct applications and even electricity production under certain circumstances. Accordingly, a three-dimensional model of a U-tube heat exchanger is simulated under both steady and unsteady conditions. Using the real field data, including the geothermal gradient and properties of each ground layer, along with the well geometry, increases the precision and accuracy of the simulation. The performance of the underground heat exchanger is studied through sensitivity analyses on the effects of working fluid inlet velocity and inlet temperature, length of the outlet pipe insulation and the U-tube diameter. According to the results of the current study, the following conclusions can be drawn:

- (a) To obtain satisfactory and reasonable results, it would be advisable to simulate the U-tube heat exchanger under unsteady state condition. The reason for this is that the decreasing trend in the ground temperature will slow down with the passage of time. Therefore, it takes a long time for the simulation to reach a steady state condition.
- (b) The great advantage of the simulated heat exchanger is that it can work steadily as a long-term geothermal production system owing to the fact that the fluid outlet temperature does not approximately change with time. For instance, in the case with fluid inlet temperature of 288.16 K and inlet velocity of 0.03 m/s , the outlet temperature is 324.73 K at the first year of operation and it declines to 324.13 K after 5 years.
- (c) It is also worth mentioning that in one case with 0.01 m pipe diameter, 303.16 K water inlet temperature and 0.5 m/s water inlet velocity, the outlet temperature reaches 114.87°C , which is suitable for electricity production. In this case, the U-tube heat exchanger is capable of producing 48.8 kW gross heat power from a single well with a geothermal gradient of 31.1°C/km .
- (d) The inlet velocity of the working fluid has a profound impact upon the performance of the U-tube heat exchanger. Indeed, except for very low velocities (i.e. below 0.03 m/s); a higher inlet velocity leads to a lower outlet temperature and a higher gross thermal power, and vice versa for lower inlet velocities.
- (e) Among diverse water inlet velocities, the optimal velocity, at which the maximum outlet temperature of 324.13 K can be attained, is 0.03 m/s at water inlet temperature of 288.16 K .

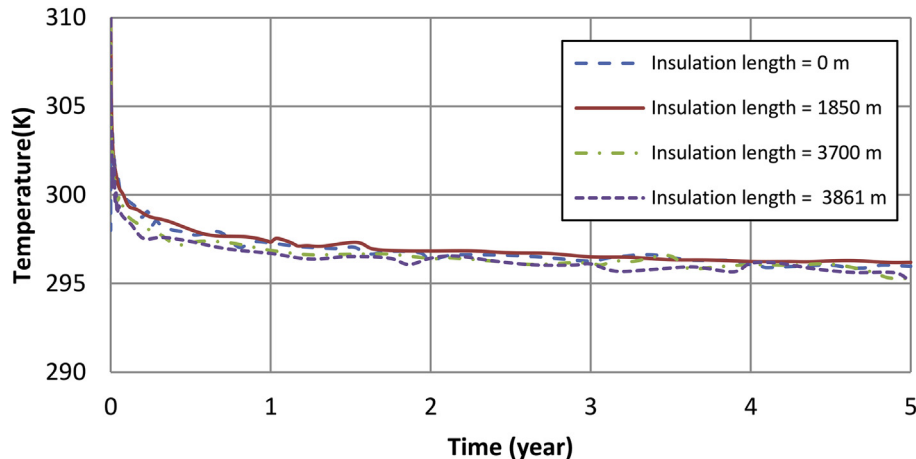


Fig. 16. Outlet temperature change with time for different insulation lengths in a case with maximum gross heat power ($U_i = 2.5 \text{ m/s}$, $T_i = 288.16 \text{ K}$).

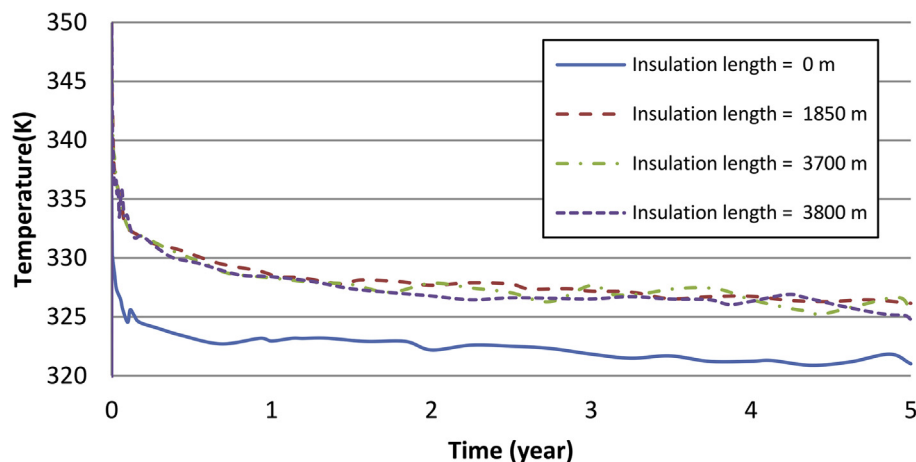


Fig. 17. Outlet temperature change with time for different insulation lengths in a case with maximum water outlet temperature ($U_i = 0.5 \text{ m/s}$, $T_i = 303.16 \text{ K}$).

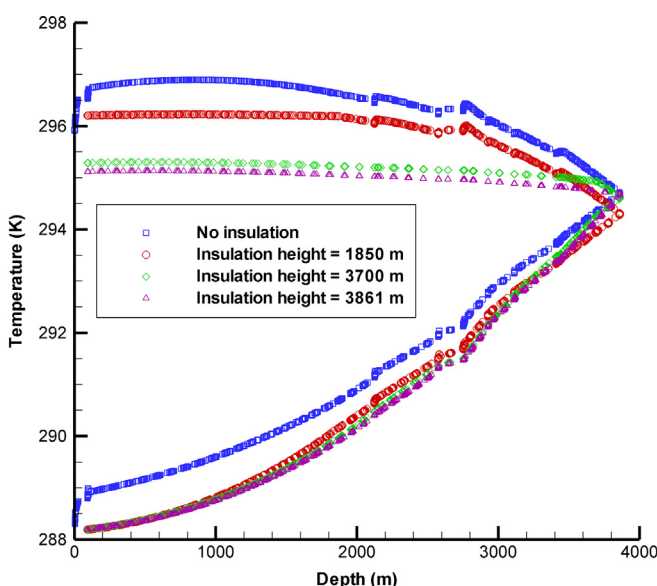


Fig. 18. Temperature variation of working fluid along the U-tube with various insulation lengths in a case with maximum gross heat power ($U_i = 2.5 \text{ m/s}$ and $T_i = 288.16 \text{ K}$).

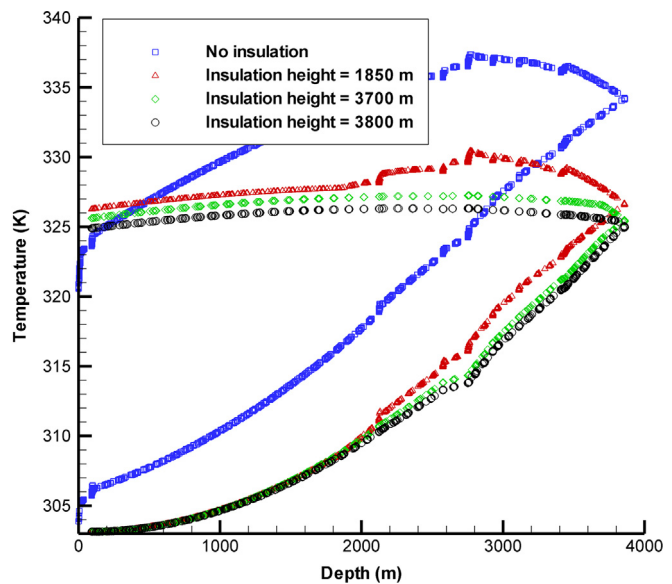


Fig. 19. Temperature variation of working fluid along the U-tube with different insulation lengths in a case with maximum water outlet temperature ($U_i = 0.5 \text{ m/s}$, $T_i = 303.16 \text{ K}$).

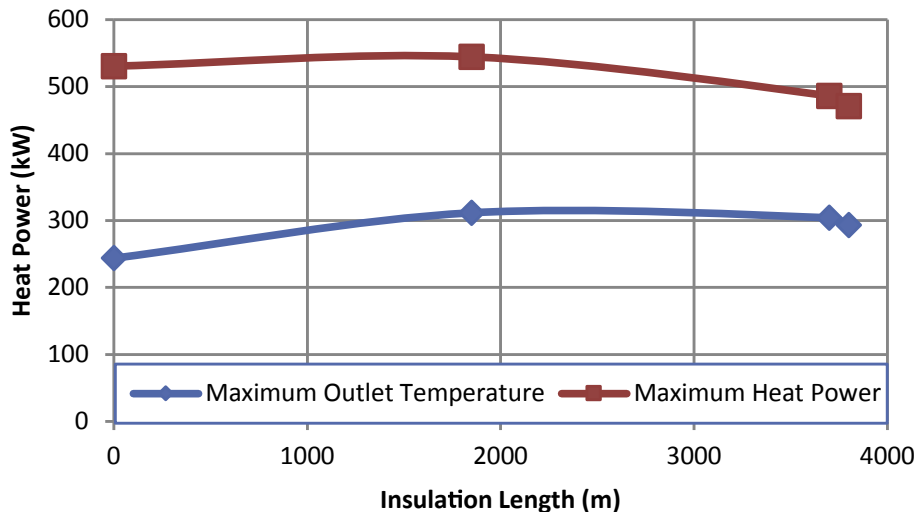


Fig. 20. Performance of the U-tube at different insulation lengths for the maximum gross heat power and fluid outlet temperature.

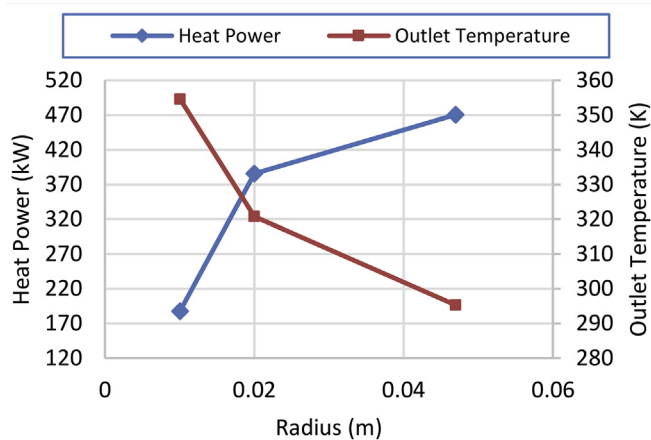


Fig. 21. Performance of the U-tube at different pipe radii after 5 years of operation for a case with maximum gross heat power ($U_i = 2.5 \text{ m/s}$ and $T_i = 288.16 \text{ K}$).

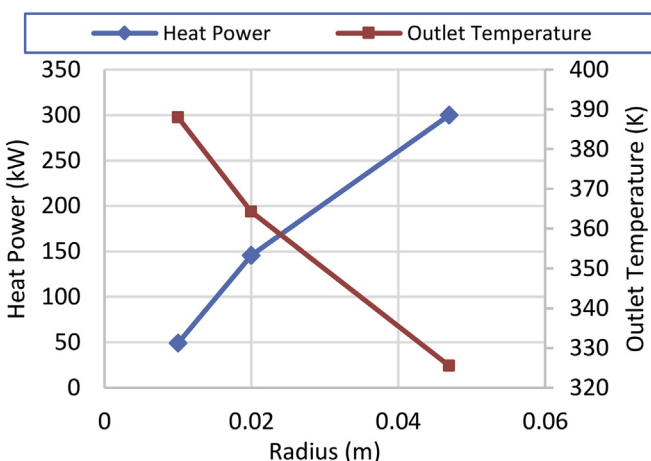


Fig. 22. Performance of the U-tube at different pipe radii after 5 years of operation for a case with maximum outlet temperature ($U_i = 0.5 \text{ m/s}$, $T_i = 303.16 \text{ K}$).

(f) As long as the water inlet temperature is lower than the bottom-hole temperature, increasing the inlet temperature

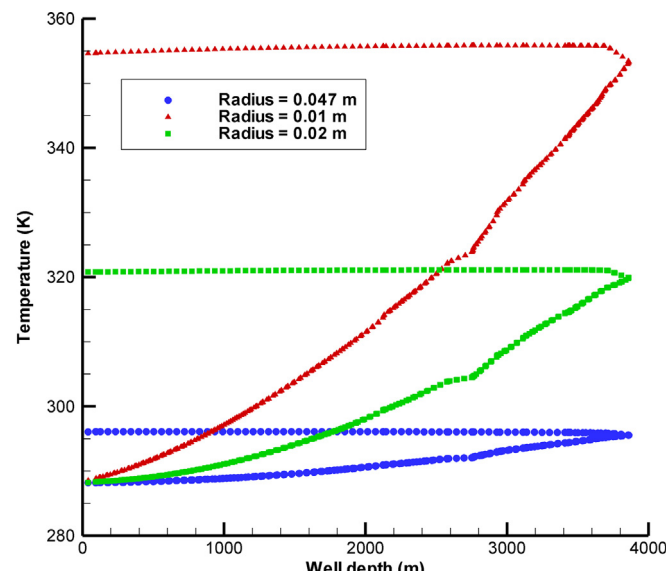


Fig. 23. Temperature variation of the working fluid along the U-tube for different pipe radii at $U_i = 2.5 \text{ m/s}$ and $T_i = 288.16 \text{ K}$.

will lead to a rise in the outlet temperature and a decline in the amount of extracted gross power.

- (g) Partial insulation on the outlet pipe is needed to effectively limit the heat loss from the ascending working fluid with a higher temperature to the portion of the surrounding ground with lower temperatures. It is also concluded that the optimum length of insulation does not almost vary with different water inlet velocities and temperatures.
- (h) The U-tube diameter is an important factor affecting the simulation results as follows:
 - At a constant inlet velocity, rising the U-tube diameter leads to decreasing the water outlet temperature and increasing the heat extraction rate.
 - At a constant mass flow rate, rising the U-tube diameter enhances the heat exchanger performance in the downward flow while it has a detrimental effect on the heat exchanger efficiency in the upward flow. For cases with a constant mass flow rate, based upon the amount of heat

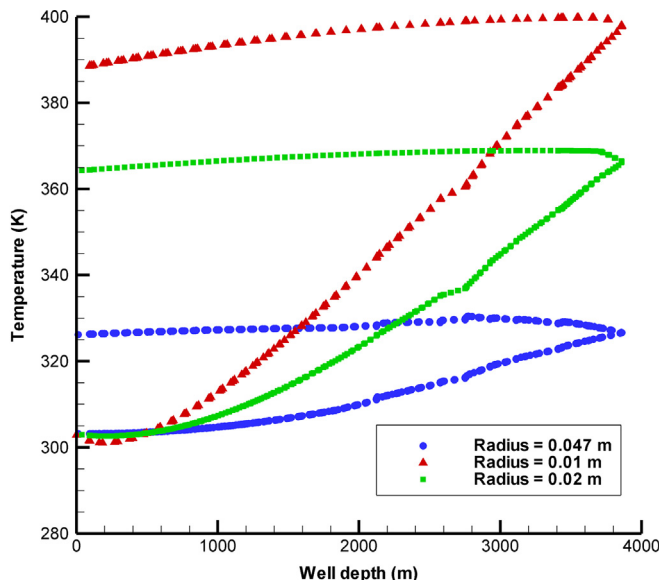


Fig. 24. Temperature variation of the working fluid along the U-tube for different pipe radii at $U_i = 0.5 \text{ m/s}$ $T_i = 303.16 \text{ K}$.

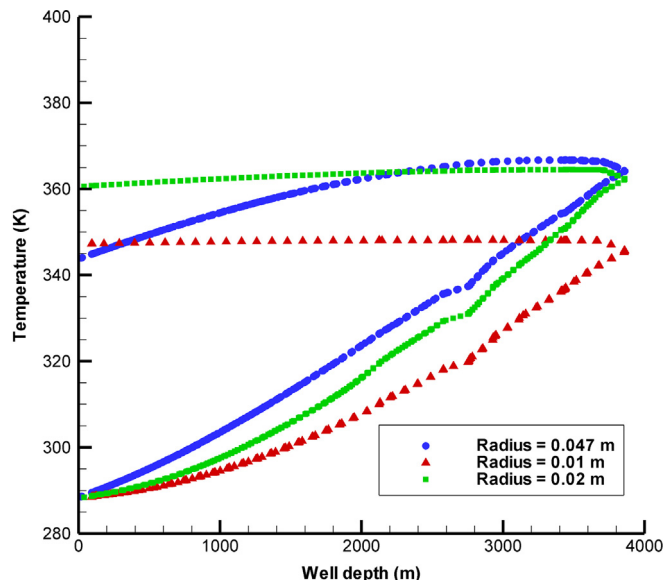


Fig. 26. Temperature variation of the working fluid with depth for different pipe radii at constant mass flow rate ($\dot{m} = 0.78 \text{ kg/s}$ and $T_i = 288.16 \text{ K}$).

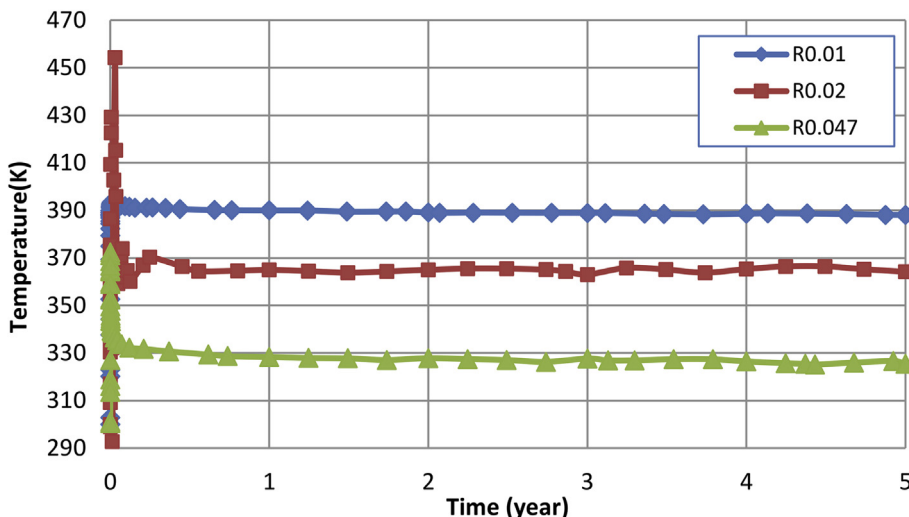


Fig. 25. Variation of water outlet temperature with time for different pipe radii at constant water inlet velocity ($U_i = 0.5 \text{ m/s}$, $T_i = 303.16 \text{ K}$).

gained through the descending fluid and the amount of heat lost through the ascending fluid, the outlet temperature may become either lower or higher as the pipe diameter increases.

Nomenclature

Variables

A	cross sectional surface (m^2)
C_1	constant used in the standard κ - ϵ model
C_2	constant used in the standard κ - ϵ model
C_3	constant used in the standard κ - ϵ model
c_p	specific heat capacity (J/kg K)
E	energy (J/kg)
G	turbulent flow production term
H_1	enthalpy of injected fluid (J/kg)
H_2	enthalpy of extracted fluid (J/kg)

h	sensible enthalpy (J/kg)
K	thermal conductivity (W/m K)
K_{eff}	effective thermal conductivity (W/m K)
\dot{m}	mass flow rate (kg/s)
p	static pressure (Pa)
\dot{Q}	heat extraction rate (W)
\vec{q}	heat flux vector
R	pipe radius (m)
S	source term
T	temperature (K)
U	fluid velocity (m/s)
Y_j	mass fraction of species j
Y_M	dilatation dissipation term

Greek letters

ε	dissipation rate of turbulent energy (m^2/s)
k	turbulent kinetic energy (m^2/s^2)

μ	dynamic viscosity (Pa s)
μ_t	turbulent viscosity (Pa s)
v	velocity (m/s)
ρ	density (kg/m^3)
σ_ε	Prandtl number of ε
σ_k	Prandtl number of k
$\bar{\tau}$	stress tensor (Pa)

Subscripts

eff	effective
i	inside
max	maximum

References

- [1] Nasruddin, et al. Potential of geothermal energy for electricity generation in Indonesia: a review. *Renew Sustain Energy Rev* 2016;53:733–40.
- [2] Gehringer M, Victor L. Geothermal handbook : planning and financing power generation. Washington, DC, USA: ESMAP; 2012.
- [3] Gallup DL. Production engineering in geothermal technology: a review. *Geothermics* 2009;38(3):326–34.
- [4] Bertani R. Geothermal power generation in the world 2005–2010 update report. In: Proceedings world geothermal congress, Bali, Indonesia; 2010.
- [5] Jalilnasrabad S, Itoi R. Flash cycle and binary geothermal power plant optimization. In: Geothermal resources council 2012 annual meeting, GRC transactions; 2012. p. 1079–84.
- [6] Cheng W-L, et al. Enhancing geothermal power generation from abandoned oil wells with thermal reservoirs. *Energy* 2016;109(Supplement C):537–45.
- [7] Bu X, Ma W, Li H. Geothermal energy production utilizing abandoned oil and gas wells. *Renew Energy* 2012;41:80–5.
- [8] Alimonti C, Soldo E. Study of geothermal power generation from a very deep oil well with a wellbore heat exchanger. *Renew Energy* 2016;86(Supplement C):292–301.
- [9] Richter A. Project in Alberta plans to tap heat in abandoned oil wells for greenhouses. 2016. Available from: <http://www.thinkgeoenergy.com/project-in-alberta-plans-to-tap-heat-in-abandoned-oil-wells-for-greenhouses/>.
- [10] Tester J, et al. The future of geothermal energy: impact of enhanced geothermal systems (EGS) on the United States in the 21st century : an assessment. Massachusetts Institute of Technology; 2006.
- [11] Kujawa T, Nowak W, Stachel AA. Utilization of existing deep geological wells for acquisitions of geothermal energy. *Energy* 2006;31(5):650–64.
- [12] Davis AP, Michaelides EE. Geothermal power production from abandoned oil wells. *Energy* 2009;34(7):866–72.
- [13] Cheng W-L, et al. Studies on geothermal power generation using abandoned oil wells. *Energy* 2013;59(Supplement C):248–54.
- [14] Noorollahi Y, et al. Numerical simulation of power production from abandoned oil wells in Ahwaz oil field in southern Iran. *Geothermics* 2015;55(Supplement C):16–23.
- [15] Caulk RA, Tomac I. Reuse of abandoned oil and gas wells for geothermal energy production. *Renew Energy* 2017;112(Supplement C):388–97.
- [16] Lee CK, Lam HN. Computer simulation of borehole ground heat exchangers for geothermal heat pump systems. *Renew Energy* 2008;33(6):1286–96.
- [17] Rees SJ. An extended two-dimensional borehole heat exchanger model for simulation of short and medium timescale thermal response. *Renew Energy* 2015;83(Supplement C):518–26.
- [18] Li Z, Zheng M. Development of a numerical model for the simulation of vertical U-tube ground heat exchangers. *Appl Therm Eng* 2009;29(5–6):920–4.
- [19] Bouhacina B, et al. Analysis of thermal and dynamic comportment of a geothermal vertical U-tube heat exchanger. *Energy Build* 2013;58(Supplement C):37–43.
- [20] Bouhacina B, Saim R, Ozturk HF. Numerical investigation of a novel tube design for the geothermal borehole heat exchanger. *Appl Therm Eng* 2015;79:153–62.
- [21] Dai LH, et al. Analysis on the transient heat transfer process inside and outside the borehole for a vertical U-tube ground heat exchanger under short-term heat storage. *Renew Energy* 2016;87(Part 3):1121–9.
- [22] Lyu Z, et al. Numerical analysis of characteristics of a single U-tube downhole heat exchanger in the borehole for geothermal wells. *Energy* 2017;125:186–96.
- [23] Ghoreishi-Madiseh SA, Hassani FP, Al-Khawaja MJ. A novel technique for extraction of geothermal energy from abandoned oil wells. In: American solar energy society (ASES); 2013. p. 1–6.
- [24] ANSYS I. ANSYS fluent tutorial guide. 2011.
- [25] Takemitsu N. An analytical study of the standard $k-\epsilon$ model. *J Fluid Eng* 1990;112(2):192–8.
- [26] Patankar SV. Numerical heat transfer and fluid flow. Hemisphere Publishing Corporation; 1980.
- [27] Batchelor GK. An introduction to fluid dynamics. Cambridge University Press; 2000.
- [28] Chieng CC, Launder BE. On the calculation of turbulent heat transport downstream from an abrupt pipe expansion. *Numer Heat Tran* 1980;3(2):189–207.
- [29] Van Doormaal JP, Raithby GD. Enhancements of the simple method for predicting incompressible fluid flows. *Numer Heat Tran* 1984;7(2):147–63.